PCCP

Effect of water/glycerol polymorphism on dynamic nuclear polarization

Journal:	*Physical Chemistry Chemical Physics*
Manuscript ID	CP-ART-01-2018-000358.R1
Article Type:	Paper
Date Submitted by the Author:	12-Mar-2018

Complete List of Authors:	Leavesley, Alisa; University of California, Santa Barbara, Chemistry and Biochemistry Wilson, Christopher; University of California, Physics Sherwin, Mark; University of California, Department of Physics Han, Songi; University of California, Department of Chemistry and Biochemistry; University of California, Department of Chemical Engineering

Effect of water/glycerol polymorphism on dynamic nuclear polarization

Alisa Leavesley[1], C. Blake Wilson[2], Mark Sherwin,[2] Songi Han[1]

[1]Department of Chemistry and Biochemistry, University of California, Santa Barbara, Santa Barbara, CA

[2]Department of Physics, University of California, Santa Barbara, Santa Barbara, CA

Abstract: A paramount feature of robust experimental methods is acquiring consistent data. However, in dynamic nuclear polarization (DNP), it has been observed that DNP-induced NMR signal enhancement of nominally the same sample can vary between different experimental sessions. We investigated the impact of various freezing conditions on the DNP results for a standard sample, 50/40/10 by volume d_8-glycerol/D_2O/H_2O solution of 40 mM 4-amino TEMPO, and found that annealing the samples 10 K above the glass transition temperature (T_g) causes significant changes to the DNP profiles and enhancements compared to rapidly frozen samples. When varying the glycerol composition to yield a solution of 60/30/10 d_8-glycerol/D_20/H_20, the DNP performance became markedly more consistent, even for samples prepared under vastly different sample freezing methods, in stark contrast with that of the 50/40/10 solution. The EPR lineshapes, T_m, and glass transition temperature, T_g, were measured under the same sample and experimental conditions as used for the DNP experiments to support the conclusion that different freezing methods change the distribution of 4-amino TEMPO radials in the 50/40/10 solution due to the formation of different polymorphs of the glass, which is mitigated in the 60/30/10 solution and is consistent with the water/glycerol vitrification literature.

1. Introduction

NMR signal enhancement via dynamic nuclear polarization (DNP) has become increasingly relevant for biological and materials studies,[1–3] where electron polarization is transferred to the surrounding nuclei upon irradiation with microwaves (μw) corresponding to the electron paramagnetic resonance (EPR) frequency.[4–7] Although research to achieve DNP at room temperature is an active field,[8,9] DNP is most commonly applied to frozen aqueous glasses at cryogenic temperatures under magic angle spinning (MAS) or static conditions.[10–13] The solvent type, sample composition, and freezing conditions will directly impact the type of glass formed, and thus the radical distribution throughout the sample.[14–16] Freed and co-workers have shown that the quality of the glass formed affects the EPR echo intensity, with better glasses producing stronger EPR signals.[16] In EPR studies of nitroxides, Kirilina and co-workers found that the size and structure of mono-radicals did not significantly influence the electron spin relaxation rates, while the solvent glass greatly influenced the electron spin relaxation rates.[17] In fact, the radical distribution in a sample can change the DNP mechanism and the maximum achievable NMR signal enhancement.[18,19] As such is it important to investigate the influence of the quality and property of vitrified glasses and their radical distribution on DNP and EPR performance.

The DNP community commonly uses water/glycerol solvent systems to form amorphous glasses upon freezing, with glycerol content ranging from 40-72% by volume, while the trademark DNP juice™ specifically refers to 60:30:10% d_8-glycerol:D_2O:H_2O.[20,21] In water/glycerol glasses, the sample volume dictates the minimum required water to glycerol ratio for effective vitrification,[14] where larger water concentrations is expected to yield inhomogeneities in the solvent system.[15] Although water/glycerol is a commonly used solvent for DNP studies, there is contention in the vitrification literature on the degree of heterogeneity occurring at the mesoscopic scale upon formation of water/glycerol glasses.[22–27] Murata and Tanka argue a liquid-liquid transition occurs, which does not affect the homogeneous macroscopic distribution of water and glycerol molecules – i.e. no macroscopic phase separation occurs, but alters their hydrogen bonding network, and thus the density of the glass formed, at the mesoscopic scale, and the system's glass transition temperature.[22,23] Feldman group proposes that at glycerol concentrations ≤ 55% vol water-water interactions prevail in addition to water-glycerol and glycerol-glycerol interactions that result in the formation of ice crystals on the mesoscopic scale with some interfacial water connecting the ice crystals and the water/glycerol domains.[24,25] The Giovambattista group agrees with the Feldman group regarding the formation of ice at low glycerol concentrations, but they disagree over the range of glycerol concentrations that this micro-phase separation occurs. They further state that the glycerol content will factor into whether the ice formed will have cubic or hexagonal structures – thus influencing the density and glass transition temperature.[26,27] The contention in the literature regarding the conditions, resultant products, and mechanism of water/glycerol vitrification are significant, but they all suggests that polymorphism exists to some degree in water/glycerol solvents, which will impact how the radicals essential for DNP and EPR are distributed in the sample. Therefore, the quality of the glass formed and the radical distribution in the glass must be known to accurately predict the ideal sample formulations to achieve large DNP enhancements, or simply consistent DNP enhancements by mitigating or utilizing solvent polymorphism.

In order to fully investigate a system used in DNP studies, a complete picture of the electron-nuclear interactions in the sample is needed. As such, it is relevant to acquire both EPR and DNP data under comparable experimental conditions.[18,19,28] Before the start of this study, we observed that the DNP enhancement for a single sample at 7 T and 4 K under static conditions varied significantly from day-to-day, by up to 40%, with a water/glycerol solution of 50:40:10 by volume d_8-glycerol/D_2O:H_2O. Thus, we investigated the glass forming conditions (freezing history and sample composition) of water/glycerol samples under static DNP conditions at 4 K, with the aim to improve the consistency and predictability of DNP enhancements. The findings of this study are relevant for other low temperature DNP operations, including MAS-DNP at 80-100 K with a commercial DNP instrument, as most water/glycerol glasses have formed by 150 K.

2. Results/Discussion

The effect of sample composition and freezing conditions were evaluated on the DNP and EPR performance and the day-to-day consistency for the commonly used water/glycerol mixture-based solvents. Two different solvent compositions of water/glycerol were tested: 541 (50:40:10) versus 631 (60:30:10) by volume of d_8-glycerol:D_2O:H_2O to make 40 mM 4-amino TEMPO (4AT) solutions. The EPR and DNP properties of each solvent composition were compared under two different freezing conditions: fast cool (FC) and thermally controlled (TC), with the two freezing histories depicted in figure 1.

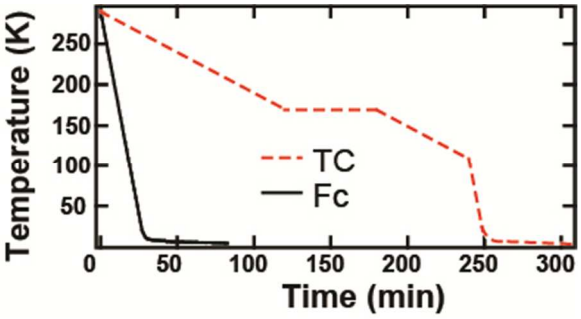

Figure 1. *Time versus temperature depiction of the two freezing conditions: fast cool (FC) 10 K/min from 290 K to 4 K [black - solid] and thermally controlled (TC) 1 K/min from 290 K to 10 K above T_g, then 1 K/min to 100 K followed 12 K/min to 4 K [red - dashed]. Temperature was monitored with a Lake Shore Cernox® temperature sensor.*

In order to understand the glassing behavior of the solvents under different freezing conditions, differential scanning calorimetry (DSC) analyses between 100 and 300 K were completed to determine their glass transition temperatures, T_g. The T_g values were determined from the second heating cycle and are shown in Table 1, while the raw DSC curves are shown in Fig. 2, where the difference in heat flow between the FC and TC freezing methods is a consequence of the cooling rate - slower cooling rates induce less heat flow. All four systems form a glass, and the glass forming transition is symmetrically observed in both the cooling and heating cycles. From this, the T_g for 631-FC, 631-TC, and 541-FC was found to be ~167.7±1.5 K, and for 541-TC the T_g is 180.4 ± 1.7 K. In the heating DSC curve of 541-FC, a crystallization and subsequent melting peaking is observed above the T_g. The finding that 631-FC, 631-TC, and 541-FC have similar T_g suggests that similar glassy matrices are ultimately formed. Only 541-TC yielded a T_g that is statistically an outlier, implying 541-TC forms a different type of glass compared to the other systems.

The differing T_g between the TC and FC freezing methods observed only for the 541 solvent agrees with the literature that suggests at ≤ 55% glycerol content, non-negligible water-water interactions prevail in addition to water-glycerol and glycerol-glycerol interactions.[24,29] We postulate that persistent water-water interactions in the 541 solvent leads to the formation of minute ice particles depending on the freezing condition, while water-water interactions are non-dominant for the 631 solvent. The crystallization and melting peaks observed in the 541-FC DSC curve support the idea that ice crystals in the 541 solvent form due to the reorganization of the hydrogen bonding network between water and glycerol above the T_g that subsequently melted — similar DSC

data have been reported by Popov and colleagues.[25] Since this thermodynamic transition is not symmetric on cooling and heating and was only observed on the heating cycle, we can say that the overall heterogeneity of the glass that formed upon cooling, according to DSC, is similar between the 631-FC/TC and 541-FC samples. However, this also shows that although 541-FC forms a similar glass as the 631 samples on cooling, there are fundamental differences in the 541 sample that allows for polymorphism to occur. This observation reiterates the influence and importance of the thermal history on water/glycerol glasses.

The reproducibility of polymorphism in frozen glasses needs to be verified in addition to the influence polymorphism has on the EPR and DNP results. If a different glassy matrix is formed with 541-TC, it is reasonable to expect that the radical distribution in the matrix would be different. This difference should be reflected in the EPR lineshape, phase memory times (T_m), and DNP spectra. These combined techniques provide insight into the bulk and local electron spin environments, where detailed descriptions of the methods and sample preparation are available in the electronic supplemental information (ESI).

Table 1. *T_g values as determined by DSC analysis of the second cycle heating curve, maximum DNP enhancements after 60 s of irradiation, ε_{60}, at 197.7 GHz of MW irradiation, and maximum EPR echo intensity for 40 mM 4-amino TEMPO when irradiated at 197.925 GHz when t_p and tau = 500 ns at 7 T and at 4 K for the different solvent compositions and freezing conditions. The echo intensities were normalized to the highest signal (631-FC). Both the DNP enhancements and the EPR echo intensities represent the average of triplicated data sets and the errors correspond to day-to-day variations, where echo intensities were not corrected for T_m.*

Sample	T_g (K)	ε_{60}
631		
TC	168.05	220 ± 20
FC	169.95	181 ± 24
541		
TC	180.35	125 ± 85
FC	164.85	143 ± 32

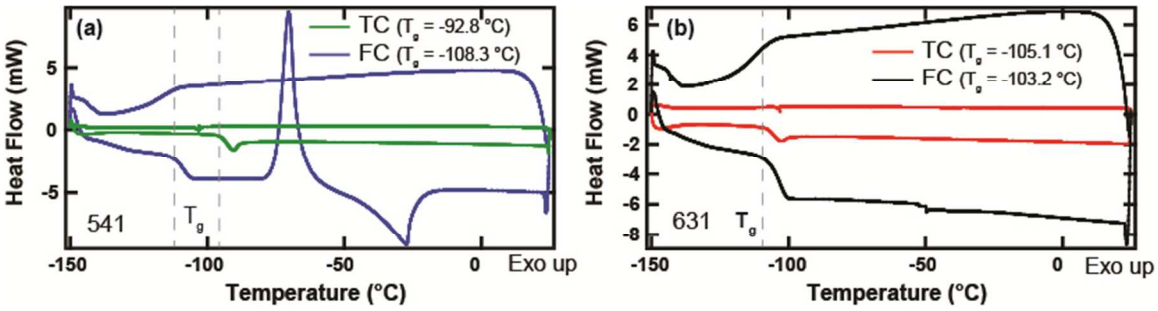

Figure 2. *DSC plots of the different freezing conditions fast cool (FC) and thermally controlled (TC) for 40 mM 4AT in 5:4:1 (a) and 6:3:1 (b) d_8-glycerol:D_2O:H_2O. The T_g from each of the heating curves are noted in the plots by dashed grey vertical lines. The cooling curves are the top curves, while the heating curves are the bottom curves. Exothermic events are up.*

The EPR lineshapes were measured to study the bulk electron spin environment, both by continuous wave (cw-) and field-swept echo detection, of the different glassing conditions and solvent compositions at 8.56 T and 240 GHz. At high magnetic fields, the lineshape of a nitroxide EPR spectrum is dictated by the g-factor anisotropy, where the principle axis system can be determined from the spectrum with g_{xx} on the low field side and g_{zz} on the high field side. The anisotropy of the hyperfine interaction between the electron spin and ^{14}N of the nitroxide will further delineate the EPR lineshape; however only the z-component of the hyperfine coupling for nitroxides is easily observable at 240 GHz. In figure 3, the 631 samples present consistent EPR lineshapes acquired by cw- and field swept echo detection for both freezing conditions. The 541 samples EPR lineshapes differ in the g_{xx} region of the spectra, where the 541-TC sample has a lower intensity g_{xx} peak that is shifted slightly lower in field by ~250 ppm, as indicated in the inset of figure 3a. The cw- EPR spectra were simulated by varying the relative ratio of two populations that differ only by their g_{xx} values, as shown in the ESI (SIfig. 1 and SITable 1). We found that the 631 and 541-FC samples all favorably populate the high field species, while 541-TC favorably populates the low field species. Independent of the solvent choice, the TC freezing method displays a slightly higher population for the low field species relative to the solvent's FC counterparts. This indicates that some (small) difference exists between the 631-TC and 631-FC systems, but that the 631 solvent is more resistant to variations in the freezing method. The consistent favoring of the high field species by 541-FC and both 631 samples corroborates the T_g data that the glass properties and radical distributions are more similar between these three samples. In contrast, there is a clear difference in the g_{xx} peak of the 541-TC sample, where differences in the radical or proton distribution due to inhomogeneities in the bulk sample would plausibly cause a shift in the g_{xx} peak (Fig. 3). It has been shown that the number of hydrogen bonds to the nitroxide moiety can shift the position of the g_{xx} peak and A_{zz}, where more hydrogen bonds shifts the g_{xx} peak to lower g-factors and smaller A_{zz}.[30,31] Thus, we speculate that the shift in the g_{xx} of 541-TC towards a lower magnetic field is caused by 541-TC having fewer average hydrogen bonds compared to the other three systems, where the observed shift of ~250 ppm is slightly larger than the loss of a single hydrogen bond – 205 ppm.[31] The difference in nitroxide-hydrogen bonds is likely due to differences in the mesoscopic structure of the glass caused by glass polymorphs; however, a rationale analysis of the hydrogen bonding network within the water/glycerol glass is outside the scope of this paper. Differences in A_{zz} could not be identified given inhomogeneous broadening of the spectra, and thus were not considered further. To determine if the change in 541-TC's g_{xx} is affected by inhomogeneities in the radical distribution, in addition to differences in the hydrogen bond network, the local electron spin concentration was evaluated for all four samples. One such method is the measurement of electron spin phase memory time, T_m, that is sensitive to the local electron spin concentration above a threshold radical concentration.[32]

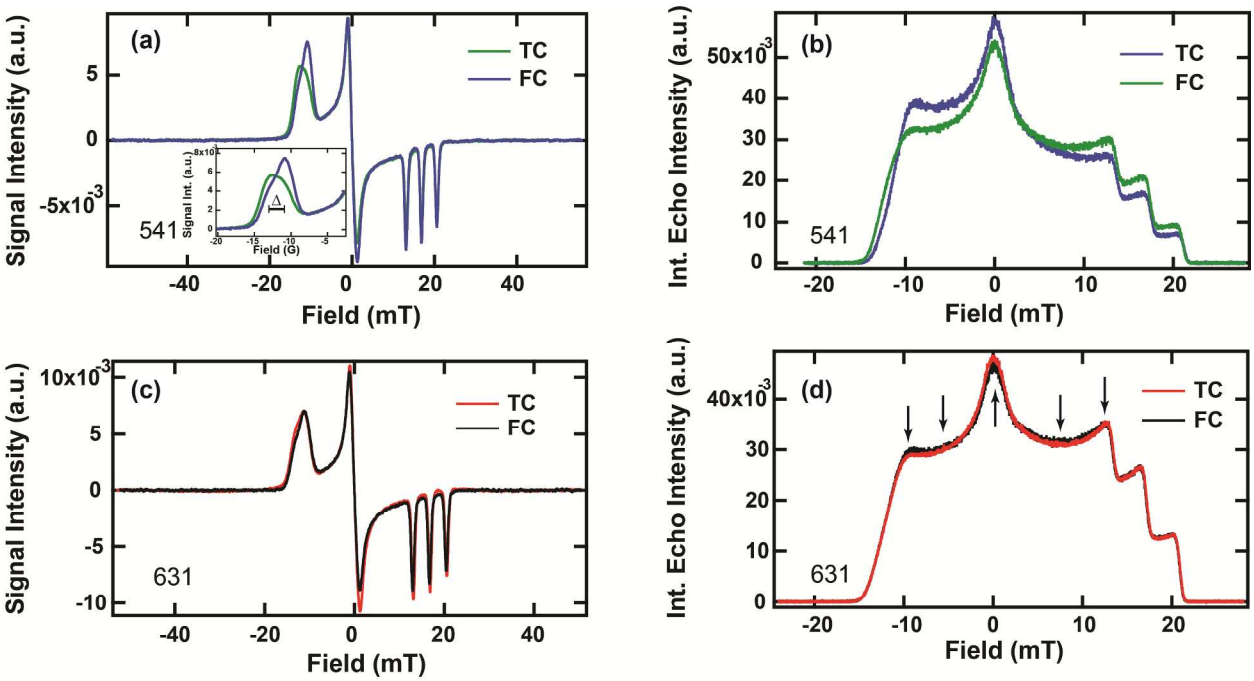

Figure 3. *EPR lineshapes of 40 mM 4AT in 5:4:1 (a,b) and 6:3:1 (c,d) d_8-gylcerol:D_2O:H_2O at 8.56 T and 4.5 K. cw-EPR (a,c) and field swept echos (b,d) are shown for both freezing conditions: fast cool (FC) and thermally controlled (TC). The inset in (a) shows the shift in g_{xx} annotated by Δ, corresponding to 250 ppm, where g_{xx} shifts from 2.00839 to 2.00787. All spectra have been normalized to the double integral. The arrows in (d) are to show the relative position of the T_m measurements in Figure 3.*

T_m was measured at five points across the EPR line (see arrows in Fig. 3d) for the different solvent compositions and freezing histories to get an overview of the local radical distributions for the entire EPR line, as T_m is sensitive to the local electron concentration. T_m measured across the EPR line accounts for distortions in the EPR spectra due to differing relaxation effects that becomes more anisotropic at high magnetic fields [33]. At 8.56 T, we found T_m to be approximately 9.5 µs across the whole EPR line for the 631-FC, 631-TC, and 541-FC samples (Fig. 4a). The 541-TC sample had distinctly shorter T_m values across the EPR line, as well as the largest anisotropy, with the shortest value of T_m, ~7.5 µs, found at the center of the EPR spectrum. T_m was also measured at 7 T to see if the trend at these two fields are consistent, and thus determine whether EPR data at 8.56 T can be used to rationalize DNP data at 7 T. To compare the T_m data at the two fields, the data was acquired at the same relative positions along the EPR line for both fields, where all the echo decays to determine T_m are shown in SIfig. 2. At 7 T, 541-FC, 631-FC, and 631-TC yield slightly smaller average T_m values compared to at 8.56 T, while 541-TC has distinctly shorter T_m (Fig. 4b). However, at 7 T all T_m values were somewhat dependent on the EPR frequency. T_m is expected to lengthen with decreasing magnetic field strength, as was observed.[33] Since similar trends in T_m are observed at 7 T and 8.56 T, the EPR lineshape analysis completed at 8.56 T can be used to support the DNP results at 7 T. Further explanation of the differences in the 7 T and 8.56 T T_m data can be found in the ESI. The similar T_m values for 631-TC, 631-FC, and 541-FC across

the entire EPR line for both magnetic fields suggest that relaxation effects did not distort the EPR spectra. The congruence between these three samples at each position implies that the average local radical distribution for each system is similar, and thus glasses with similar radical heterogeneity are formed.[34] The anisotropy observed for the 541-TC system suggests a heterogeneous glass was formed, since different glass types can alter relaxation rates.[17] Analysis of T_m can be taken a step further as stated by Edwards et al, who show that the temperature dependence of T_m below the Zeeman temperature – here 9.7 K – is modulated by the electron flip-flop rate above a threshold radical concentration (~1 mM).[32] This electron flip-flop rate is dependent on the electron-electron dipolar interactions between the non-irradiated electron spins, which follow an r^3 dependence.[32] The radical concentration is extracted based on the average inter-radical distance for a given concentration. Therefore, longer T_m values correlate to shorter electron flip-flop rates and longer average distances between nearest neighboring radicals.[32] Thus, the finding that the 541-TC system at 4 K yields shorter T_m values across the entire EPR line at 7T and 8.56 T, specifically around the center of the EPR line, where the electron spin population is greatest, implies the presence of regions with higher effective radical concentrations compared to the other three systems.[32] In other words, the radicals in the 541-TC system are clustering, resulting in a more heterogeneous radical distribution than in the other three samples, which is likely caused by 541-TC forming different glass polymorphs.

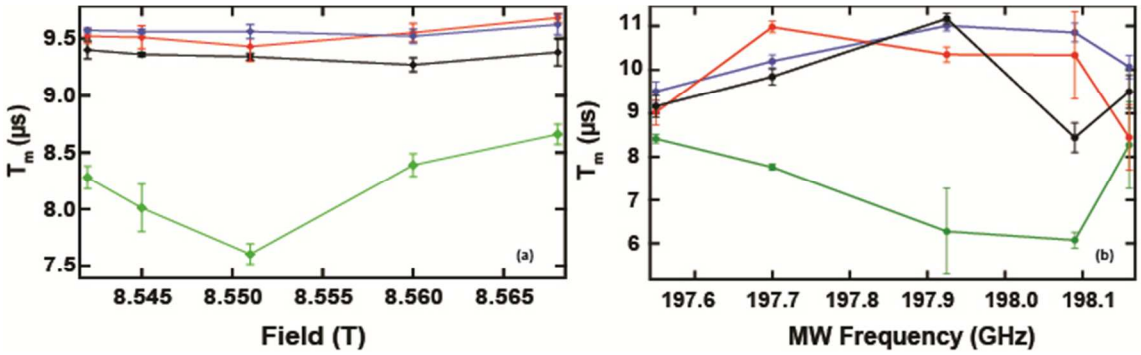

Figure 4. T_m was plotted as a function of the relative position along the EPR line as indicated in figure 2d for the different freezing conditions and model solutions of 40 mM 4AT as defined by the color code inside the plot, where (a) indicates T_m measured at 4.5 K and at 8.56 T (240 GHz) and (b) indicates T_m measured at 4 K and at 7 T (198 GHz). Lines are drawn to guide the eye.

The effect of glass polymorphism on the DNP performance was examined through the maximum NMR signal enhancement ($\varepsilon_{60}=S_{on,60}/S_{off,eq}$) and the DNP spectra—DNP enhancement as a function of the µw irradiation frequency. DNP spectra were taken in triplicates to compare the average enhancements in the different glassy matrices of the samples. Their consistency over multiple days is shown as error bars in figure 5, with representative spectra for each system shown in the ESI (SIfig. 3). The 631-FC and 631-TC DNP spectra are similar to each other, with the measurable NMR signal enhancements occurring within the frequency span

of the allowed EPR transitions and a peak-to-peak frequency difference of ~400 MHz. The 631-FC DNP spectrum is slightly broader than the 631-TC spectrum. The 541-TC spectrum differed significantly from the 541-FC spectrum with a broader spectrum near the baseline and a peak-to-peak frequency difference of ~500 MHz compared to the ~400 MHz of the 541-FC spectrum, as well as a ~ 20% smaller negative enhancement. In fact, the 541-TC sample displayed such large variations in the day-to-day signal enhancements that we cannot conclude whether the 541-TC yields larger or smaller enhancements relative to 541-FC sample, even after comparing more than six data sets, where ε_{60} ranged from 40 to 210. The ε_{60} were determined in reference to steady state NMR signal without MW irradiation, where T_{1n} was assumed to be the same for all systems as the global radical concentration is the same. This effectively means that all ε_{60} were scaled equally, but it does not account for any differences in nuclear relaxation rates due to radical clustering. The 631-TC sample showed the least day-to-day variability, and yielded the largest overall ε_{60} by 15-20% relative to the 181 signal enhancement observed for 631-FC as noted in table 1, where the reported values are the average ε_{60} and the error represents the standard deviation of the day-to-day variation. The 631-FC sample was the second best in terms of yielding large and consistent signal enhancements. Even though the distribution of radicals between the 631-FC and 631-TC systems is similar according to T_m, and the overall glass property is similar according to the T_g from DSC, DNP studies illuminate the existence of heterogeneities even between 631 samples with different freezing histories, although simulated EPR spectra did hint at this. These results show that DNP is sensitive to the arrangement of the nuclear spins, as well as the electron spins in the glassy matrix as dictated by glass polymorphism, but differentiating between the different factors is beyond the scope of this study. It becomes clear that predicting DNP enhancement values is significantly more challenging than rationalizing the EPR lineshapes, T_m data, or the shape of the DNP profile, as explaining DNP enhancements will require an in-depth understanding of the entire nuclear and electron spin ensemble of the sample.[18] Notably, 631-TC yields the highest DNP enhancement but also the weakest EPR signal intensity and requires ~4 hours to freeze the sample, while 631-FC yields both good DNP enhancements and EPR echo intensities, and only takes ~2 hours to freeze the sample.

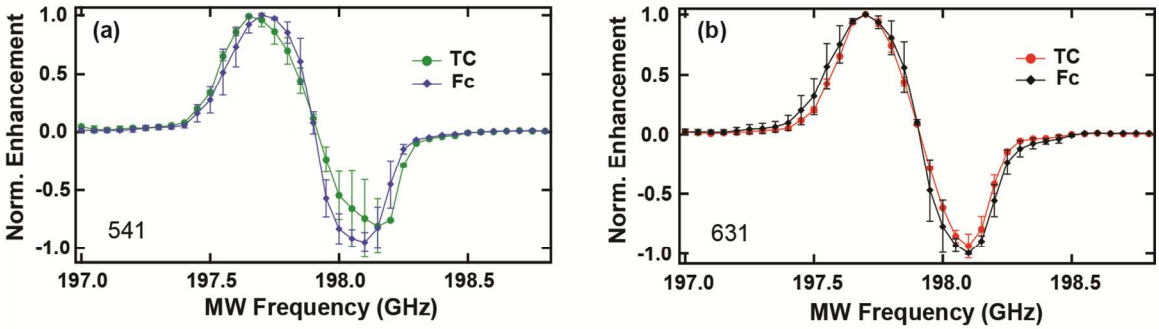

Figure 5. Normalized average DNP profiles comparing the freezing conditions (FC and TC) of 40 mM 4AT in 5:4:1 (a) and 6:3:1 (b) d_8-gylcerol:D_2O:H_2O taken at 7 T and 4K. All spectra were normalized to the maximum

signal intensity and standard deviations are shown to indicate the variability from day-to-day for the triplicated datasets. Lines are drawn to guide the eye.

The variability of the 541-TC sample and the larger DNP signal enhancement found with the 631-TC sample is consistent with the TC freezing resulting in clustering of the radicals, which is partially mitigated by the 631-TC sample forming a better glass. In order to test this hypothesis, we evaluate a sample that contains a low radical concentration of 5 mM, where a homogeneous distribution of the radicals would yield an average inter-radical distance of 3.75 nm. A sample with this range of inter-radical separation should yield a distinct DNP spectrum and DNP power curve (DNP signal enhancement as a function of applied μw irradiation power) corresponding to the solid effect (SE) DNP mechanism. If radical clustering occurs during glass formation of the 541 solvent with a TC freezing history, then the DNP profiles of 5 mM 4AT should no longer be purely dominated by the SE. Indeed, the influence of the freezing history on the radical distribution in water/glycerol glasses can be observed in the DNP spectra of 5 mM 4AT with a 541 solvent composition. The 541-FC sample shows a broader DNP spectrum near the baseline with a peak-to-peak DNP frequency of 450 MHz compared to 400 MHz observed for the 541-TC sample (Fig. 6a). Neither sample exhibits a classic SE DNP spectral lineshape; however, the differences in the DNP spectra are consistent with 541-FC having a larger SE contribution than that of the 541-TC sample.[18,19] (See ESI for discussion on the effect of the DNP mechanism on the DNP spectra.) A comparison of DNP spectra of the 5 mM 4AT samples with the 40 mM 4AT 541-FC is shown in SIfigure 4 to illustrate the larger cross effect (CE) mechanistic contribution for the 5 mM TC sample. The larger CE contribution observed in the DNP spectrum of 541-TC shows that radical clustering must be present, effectively increasing the local radical concentration induced by glass polymorphism in the 541 solvent above the nominal 5 mM. This hypothesis is corroborated by the T_m measured for the 5 mM 4AT samples at 7 T to be 9.2 μs and 14.5 μs in the 541-TC and 541-FC samples, respectively. As discussed, the shorter T_m for TC implies a higher local radical concentration compared to FC. The DNP power curves show that the 541-TC yielded larger signal enhancements than the 541-FC sample (Fig. 6b). This is consistent with the hypothesis of radical clustering and glass polymorphism occurring in 541-TC, given that the CE is more efficient than the SE in polarizing nuclei, which results in larger signal enhancements.[18,19]

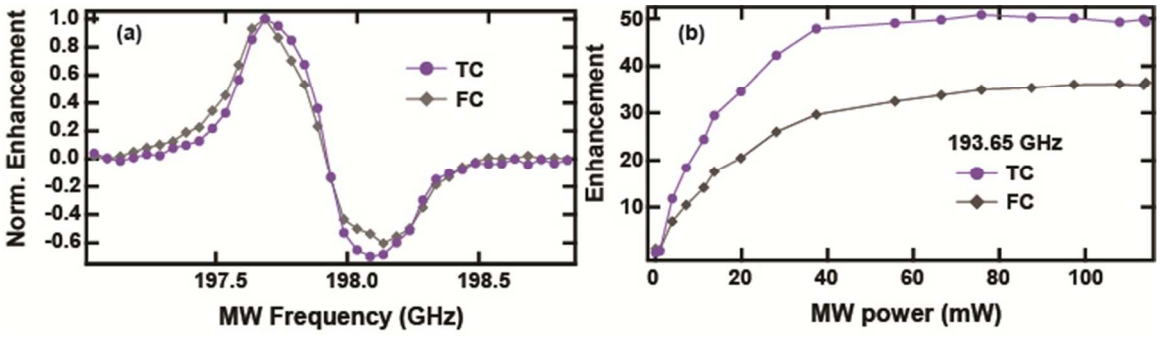

Figure 6. Normalized DNP profiles comparing the freezing conditions (FC and TC) of 5 mM 4AT in 5:4:1 (a) and the power curves of the same sample obtained at 193.65 GHz of MW irradiation (b) at 4 K and 6.95 T. The DNP profiles were normalized to the maximum of the signal intensity and the frequency was scaled by 4 GHz to represent data acquired at 7 T for comparison to the rest of the data presented here. Lines are drawn to guide the eye.

3. Conclusions

The analysis of DSC, EPR lineshape, T_m, and DNP spectral data shows that water/glycerol glasses with < 60 %v/v of glycerol are prone to solvent polymorphism upon freezing below 150 K that affect the performance and reproducibility of the resulting DNP and EPR data. We provide a mechanistic basis for why the 631 solvent provides more consistent DNP performance from day-to-day by minimizing glass polymorphism, relatively independent of the freezing method. The TC freezing method for 631 resulted in a 15-20% (when considering day-to-day variations) improvement on ^{1}H signal enhancement by DNP for our model system at 4 K, due to a slight increase in the local radical concentration, even though this was not detectable by T_m. The TC freezing method may be beneficial for some systems where every feasible improvement on signal enhancement is necessary or desired. If maximal signal enhancement is not necessary, then a faster cooling method, such as FC is recommended to save experimental time. Although some users prepare samples via rapid quenching in liquid nitrogen, which should improve the quality of the glass formed, not all sample or hardware systems are compatible with this vitrification method.

The consistency between the EPR lineshape, T_m, and DNP results shows that EPR is a critical evaluation metric for DNP, where variation in DNP performance can be understood and rationalized by EPR analyses, however only to a certain degree. The residual day-to-day variation, with larger variations observed for the 541 solvent composition, is a function of the freezing/thermal histories of each sample. Although the 541 solvent has a propensity to form glass polymorphs, the freezing method will determine the degree to which polymorphism and radical heterogeneity occurs. Thus, we reiterate the importance of the solvent thermal history, which can induce greater polymorphism, especially if the glycerol content in a water/glycerol glass is ≤ 55%, as in 541, and/or is combined with thermal annealing, as defined by TC in this study. Perhaps not surprisingly, the empirically optimized and widely used solvent for cryogenic DNP, DNP juice^{TM}, has glycerol content of 60%, which provides the most reproducible DNP and EPR results independent of freezing history.[35,36] For all that the 631 solvent yields consistent EPR spectra, T_m, and DNP spectral lineshapes, consistent day-to-day DNP signal enhancement persists as the hardest parameter to achieve. This is because the spatial arrangement of the *entir*e electron and nuclear spin ensemble of the sample contributes to the DNP performance that may show variation, even if globally and qualitatively comparable glasses are formed. Thus, there is still significant development efforts needed to rationalize and predict the complete DNP performance.

4. Acknowledgments

We would like to thank Rachel Behrens and the MRL Polymer group for their help with DSC. This material is based upon work supported by the National Science Foundation (CHE #1505038, MCB #1617025, and MCB #1244651) and the Binational Science Foundation (Grant #2014149).

5. References

1 D. A. Hirsh, A. J. Rossini, L. Emsley and R. W. Schurko, *Phys. Chem. Chem. Phys.*, 2016, **18**, 25893–25904.

2 L. Protesescu, A. J. Rossini, D. Kriegner, M. Valla, A. De Kergommeaux, M. Walter, K. V. Kravchyk, M. Nachtegaal, J. Stangl, B. Malaman, P. Reiss, A. Lesage, L. Emsley, C. Copéret and M. V. Kovalenko, *ACS Nano*, 2014, **8**, 2639–2648.

3 B. J. Wylie, B. G. Dzikovski, S. Pawsey, M. Caporini, M. Rosay, J. H. Freed and A. E. McDermott, *J. Biomol. NMR*, 2015, **61**, 361–367.

4 C. T. Farrar, D. a. Hall, G. J. Gerfen, S. J. Inati and R. G. Griffin, *J. Chem. Phys.*, 2001, **114**, 4922–4933.

5 Y. Hovav, A. Feintuch and S. Vega, *J. Magn. Reson.*, 2010, **207**, 176–189.

6 Y. Hovav, A. Feintuch and S. Vega, *J. Magn. Reson.*, 2012, **214**, 29–41.

7 D. Shimon, Y. Hovav, A. Feintuch, D. Goldfarb and S. Vega, *Phys. Chem. Chem. Phys.*, 2012, **14**, 5729–5743.

8 A. Zagdoun, G. Casano, O. Ouari, M. Schwarzwälder, A. J. Rossini, F. Aussenac, M. Yulikov, G. Jeschke, C. Coperet, A. Lesage, P. Tordo and L. Emsley, *J. Am. Chem. Soc.*, 2013, **135**, 12790–12797.

9 Ü. Akbey, A. H. Linden and H. Oschkinat, *Appl. Magn. Reson.*, 2012, **43**, 81–90.

10 D. Lee, E. Bouleau, P. Saint-Bonnet, S. Hediger and G. De Paëpe, *J. Magn. Reson.*, 2016, **264**, 116–124.

11 D. Sezer, M. J. Prandolini and T. F. Prisner, *Phys. Chem. Chem. Phys.*, 2009, **11**, 6626–6637.

12 B. Vuichoud, J. Milani, A. Bornet, R. Melzi, S. Jannin and G. Bodenhausen, *J. Phys. Chem. B*, 2014, **118**, 1411–1415.

13 R. E. Hurd, Y. F. Yen, A. Chen and J. H. Ardenkjaer-Larsen, *J. Magn. Reson. Imaging*, 2012, **36**, 1314–1328.

14 V. Berejnov, N. S. Husseini, O. A. Alsaied and R. E. Thorne, *J. Appl. Crystallogr.*, 2006, **39**, 244–251.

15 D. Banerjee and S. V. Bhat, *J. Non. Cryst. Solids*, 2009, **355**, 2433–2438.

16 E. R. Georgieva, A. S. Roy, V. M. Grigoryants, P. P. Borbat, K. A. Earle, C. P. Scholes and J. H. Freed,

J. Magn. Reson., 2012, **216**, 69–77.

17 E. P. Kirilina, I. A. Grigoriev and S. A. Dzuba, *J. Chem. Phys.*, 2004, **121**, 12465.

18 A. Leavesley, D. Shimon, T. A. Siaw, A. Feintuch, D. Goldfarb, S. Vega, I. Kaminker and S. Han, *Phys. Chem. Chem. Phys.*, 2017, **19**, 3596–3605.

19 T. a. Siaw, M. Fehr, a. Lund, a. Latimer, S. a. Walker, D. T. Edwards and S. Han, *Phys. chem. chem. phys.*, 2014, **16**, 18694–18706.

20 D. Lee, S. Hediger and G. De Paëpe, *Solid State Nucl. Magn. Reson.*, 2015, **66–67**, 6–20.

21 D. A. Hall, D. C. Maus, G. J. Gerfen, S. J. Inati, L. R. Becerra, F. W. Dahlquist and R. G. Griffin, *Science (80-.).*, 1997, **276**, 930–932.

22 K. Murata and H. Tanaka, *Nat. Mater.*, 2012, **11**, 436–443.

23 K. Murata and H. Tanaka, *Nat. Commun.*, 2013, **4**, 1–8.

24 Y. Hayashi, A. Puzenko, I. Balin, Y. E. Ryabov and Y. Feldman, *J. Physcial Chem. B*, 2005, **109**, 9174–9177.

25 I. Popov, A. Greenbaum (Gutina), A. P. Sokolov and Y. Feldman, *Phys. Chem. Chem. Phys.*, 2015, **17**, 18063–18071.

26 D. A. Jahn, J. Wong, J. Bachler, T. Loerting and N. Giovambattista, *Phys. Chem. Chem. Phys.*, 2016, **18**, 11042–11057.

27 J. Bachler, V. Fuentes-Landete, D. A. Jahn, J. Wong, N. Giovambattista and T. Loerting, *Phys. Chem. Chem. Phys.*, 2016, **18**, 11058–11068.

28 Y. Hovav, D. Shimon, I. Kaminker, A. Feintuch, D. Goldfarb and S. Vega, *Phys. Chem. Chem. Phys.*, 2015, **17**, 6053–6065.

29 A. Puzenko, Y. Hayashi, Y. E. Ryabov, I. Balin, Y. Feldman, U. Kaatze and R. Behrends, *J. Phys. Chem. B*, 2005, **109**, 6031–6035.

30 E. Bordignon, A. I. Nalepa, A. Savitsky, L. Braun and G. Jeschke, *J. Physcial Chem. B*, 2015, **119**, 13797–13806.

31 E. Bordignon, H. Brutlach, L. Urban, K. Hideg, A. Savitsky, A. Schnegg, P. Gast, M. Engelhard, E. J. J. Groenen, K. Möbius and H. J. Steinhoff, *Appl. Magn. Reson.*, 2010, **37**, 391–403.

32 D. T. Edwards, S. Takahashi, M. S. Sherwin and S. Han, *J. Magn. Reson.*, 2012, **223**, 198–206.

33 E. P. Kirilina, T. F. Prisner, M. Bennati, B. Endeward, S. A. Dzuba, M. R. Fuchs, K. Möbius and A. Schnegg, *Magn. Reson. Chem.*, 2005, **43**, 119–129.

34 H. Sato, V. Kathirvelu, G. Spagnol, S. Rajca, A. Rajca, S. S. Eaton and G. R. Eaton, *J. Phys. Chem. B*, 2008, **112**, 2818–2828.

35 G. Mathies, M. A. Caporini, V. K. Michaelis, Y. Liu, K. Hu, D. Mance, J. L. Zweier, M. Rosay, M. Baldus and R. G. Griffin, *Angew. Chemie - Int. Ed.*, 2015, **54**, 11770–11774.

36 A. B. Barnes, M. L. Mak-Jurkauskas, Y. Matsuki, V. S. Bajaj, P. C. A. van der Wel, R. DeRocher, J. Bryant, J. R. Sirigiri, R. J. Temkin, J. Lugtenburg, J. Herzfeld and R. G. Griffin, *J. Magn. Reson.*, 2009, **198**, 261–270.